Optics Letters

Broadband on-chip near-infrared spectroscopy based on a plasmonic grating filter array

Erwen Li, Xinyuan Chong, Fanghui Ren, and Alan X. Wang*

School of Electrical Engineering and Computer Science, Oregon State University, Corvallis, Oregon 97331, USA
**Corresponding author: wang@eecs.oregonstate.edu*

Received 23 February 2016; revised 20 March 2016; accepted 21 March 2016; posted 22 March 2016 (Doc. ID 259898); published 19 April 2016

We demonstrate an ultra-compact, broadband on-chip near-infrared (NIR) spectroscopy system based on a narrow-band plasmonic filter array. The entire filter array, consisting of 28 individual subwavelength metallic gratings, was monolithically integrated in a thin gold film on a quartz substrate, covering a 270 nm spectra from 1510 nm to 1780 nm. In order to achieve a high spectral resolution, extremely narrow slits are created for the gratings with a polymer waveguide layer on top, generating narrow-band guided-mode resonances through coupling with the surface-plasmon resonances of the metallic gratings. Experimental results show that the transmission bands of the filter array have full width at half-maximum of only 7 nm–13 nm, which is sufficient for NIR spectroscopy. The NIR absorption spectroscopy of xylene using the on-chip plasmonic filter array matches very well with the results from conventional Fourier transform infrared spectroscopy, which proves the great potential for NIR sensing applications. © 2016 Optical Society of America

OCIS codes: (130.7408) Wavelength filtering devices; (050.1950) Diffraction gratings; (300.6340) Spectroscopy, infrared; (310.6628) Subwavelength structures, nanostructures.

http://dx.doi.org/10.1364/OL.41.001913

Infrared (IR) absorption spectroscopy is widely accepted as a reliable technique for chemical and biological sensing. Since IR spectroscopy is based on detecting analytes' unique molecule vibration modes, it has the advantages of multiplexing and label-free sensing. These advantages make this technique more attractive than other optical techniques such as fluorescence or refractive index sensing [1,2]. In past years, many miniaturized on-chip IR sensors have been reported [3–7]. However, many of them still rely on commercially available IR spectroscopy systems, such as Fourier transform infrared (FT-IR) spectroscopy [8] and tunable diode laser absorption spectroscopy (TDLAS) [9], which are expensive and bulky desktop instruments. Due to the urgent need of field testing and on-site sensing, the demand for developing a portable, cost-effective IR spectroscopy system is continuously growing. Therefore, an on-chip IR spectrometer is highly desired. In past years, several on-chip spectroscopy methods have been reported, including arrayed waveguide grating (AWG) [10–12], echelle diffraction grating (EDG) [13,14], superprism-based photonic crystal [15], microresonator array [16], and filter array based on Fabry–Perot (FP) cavities [17,18]. However, these techniques suffer from the compromise between spectral resolution and operating bandwidth, which limits their practical applications. Besides, many of these on-chip spectrometers require sophisticated optical coupling methods, such as grating couplers [12] or lensed fibers, [14] to couple light into the submicron scale waveguides, or delicate Micro-electro-mechanical systems (MEMS) [17] to control the spectroscopy, which limits their use in field sensing.

Subwavelength grating nanostructures have attracted great attention due to their unique ability to manipulate light [19,20]. A variety of optical devices have been reported using subwavelength gratings including polarizers, wide-band reflectors, narrow-band filters, and even optical modulators [21,22]. Particularly, guided-mode resonance (GMR) filters, consisting of dielectric subwavelength gratings with a waveguide layer, can be designed to act as narrow-band reflection filters, which can achieve linewidths less than 1 nm and nearly 100% efficiency at the resonance wavelength [20]. The resonance peak can be simply tuned by shifting the grating period, offering the possibility to incorporate multiple GMR filters for spectroscopy. Liu *et al.* reported a new kind of discrete frequency IR (DF-IR) spectrometer working in the mid-infrared spectral region based on narrow-band reflection GMR filters [23]. However, such GMR filters require large grating areas to achieve the theoretical performance [24], and complex optical setup to work at the reflection mode. On the other hand, ultra-compact subwavelength metallic grating structures, based on surface-plasmon resonances (SPRs), are often used as efficient transmission color filters [25–28]. Compared with a reflection filter, a transmission band-pass filter requires a simpler setup, which is more suitable for compact spectroscopy systems. However, a simple plasmonic grating filter is not suitable for spectroscopy due to its relatively large transmission bandwidth. Recently, studies show that through combining GMRs and SPRs, metallic grating can also be used to design a narrow-band band-pass filter [29] with a waveguide layer.

In this Letter, we developed a new type of ultra-compact on-chip spectrometer, which employs a narrow-band plasmonic

grating band-pass filter array as a wavelength-selective component for IR spectroscopy, achieving a high spectral resolution around 10 nm and wide operating bandwidth over 270 nm in NIR wavelength range from 1510 nm to 1780 nm. The high-efficiency narrow-band plasmonic filters were integrated onto a single chip with total size of only 1.5 mm^2. By measuring the transmitted optical power of each filter under normal incident from a broadband light source, we extract the NIR spectral information of xylene, a volatile organic compound (VOC), which quantitatively matches the FT-IR measurement results.

The structure consists of a gold grating layer with an array of ultra-narrow slits on a quartz substrate, covered by a thin layer of UV-cured SU-8 photoresist, as represented in Fig. 1(a). The refractive index of the SU-8 layer ($n_{SU8} = 1.57$) is greater than that of the quartz substrate ($n_{subs} = 1.45$), which makes the SU-8 thin film act as a waveguide layer in this structure. When a TM-polarized wave is incident on the structure, surface plasmon resonances (SPRs) are excited at the gold/SU-8 interface, and are coupled with narrow-band guided-mode resonances (GMRs) supported by the waveguide layer. The GMR, which is also called the leaky mode, induces a narrow transmission peak at the phase matching condition $k_{\|} = \beta \pm 2\pi m/\Lambda$, where $k_{\|}$ is the in-plane wavevector of the incident light and $k_{\|} = 0$ for normal incidence, β is the propagation constant of the guided mode, and m is the diffraction-order index. The parameters that can be modified based on design are the gold layer thickness d_{Au}, the gold slit width w, the waveguide layer thickness d_{wg}, and the grating period Λ. In our design, multiple filters are single-chip integrated. Therefore, d_{Au}, w, and d_{wg} are chosen to be the same value for all filters. The peak transmission wavelengths of each filter are tuned by Λ. Optimization of these parameters is performed by the DiffractMOD of RSoft photonic component design suite, which is based on rigorous coupled-wave analysis (RCWA). Although the optimized parameters for each filter aimed at different wavelengths may be different, a comprehensive consideration of the filter efficiency, spectral width, and side-band transmission for the entire wavelength range determines $d_{Au} = 40$ nm, $w = 120$ nm, and $d_{wg} = 1.35$ μm. Filters with Λ ranging from 973 nm to

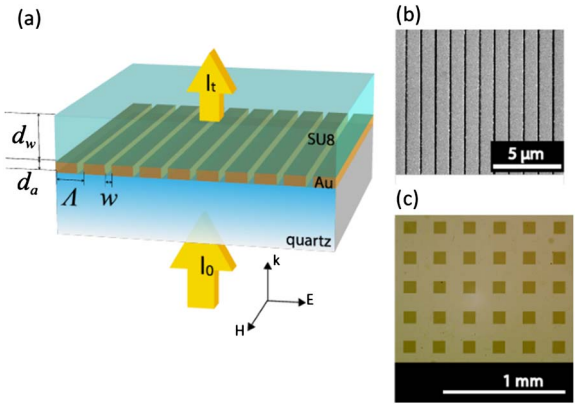

Fig. 1. (a) Schematic of a plasmonic metallic grating filter. For geometrical parameters, d_{Au} is the gold layer thickness, w is the gold slit width, d_{wg} is the waveguide layer thickness, and Λ is the grating period. I_0 and I_t stand for the intensity of the incident and transmitted light waves. (b) Scanning electron microscopy (SEM) image of one fabricated gold grating after FIB. (c) Optical image of the fabricated filter array.

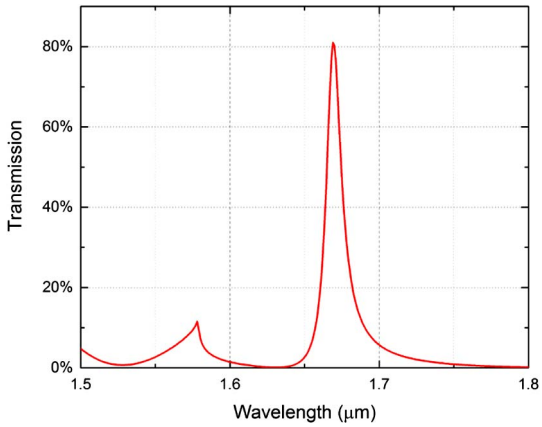

Fig. 2. Simulated transmission spectrum of one designed filter ($\Lambda = 1.089$ μm).

1157 nm provide bandwidth covering wavelengths from 1510 nm to 1780 nm. The calculated transmission spectrum of a 1.67 μm band-pass filter under normal incidence for a TM-polarized wave is presented in Fig. 2, when $\Lambda = 1.089$ μm. The filter efficiency approaches 81%, and full width at half-maximum (FWHM) is 12 nm.

We must point out that beside the main peak generated by the plasmonic filter, there is a small side peak at shorter wavelength to the main peak, which is due to the Rayleigh anomaly [30,31]. The existence of the side peak will affect the accuracy of the on-chip spectrometer. In this Letter, we developed a numerical method to suppress the side peak. Now let's consider the transmission spectrum of one filter, which can be expressed as

$$f_{\text{filter},i}(\lambda) = f_{\text{sideband},i}(\lambda) + f_{\text{ideal},i}(\lambda), \quad \textbf{(1)}$$

in which $f_{\text{filter},i}(\lambda)$ represents the spectrum of the ith filter with transmission peak at wavelength λ_i and FWHM $\delta\lambda_i$, $i = 1, 2, \ldots 28$, $f_{\text{ideal},i}(\lambda)$ represents the spectrum of an ideal filter with the same corresponding λ_i and $\delta\lambda_i$, while without the side band, and $f_{\text{sideband},i}(\lambda)$ represents the difference of the spectra between an ideal and a real filter. Because our filter array covers the entire desired bandwidth, there are a series of corresponding ideal filters that cover the same bandwidth. Using these ideal filters as the basic elements, we can express our real filters as

$$f_{\text{filter},i}(\lambda) \approx \sum_{j=1}^{28} A_{ij} f_{\text{ideal},j}(\lambda), \quad \textbf{(2)}$$

in which A_{ij} is the coefficient, $i, j = 1, 2, \ldots 28$. Accordingly, given the spectra of our filter array, we can calculate the spectra of the idea filters

$$[f_{\text{ideal},i}(\lambda)] \approx [A_{ij}]^{-1}[f_{\text{filter},j}(\lambda)]. \quad \textbf{(3)}$$

Integrating the spectra over wavelength, we get the relationship between measured transmitted power of filters and power of corresponding ideal filters

$$[I_{\text{ideal},i}] \approx [A_{ij}]^{-1}[I_{\text{filter},j}], \quad \textbf{(4)}$$

in which $I_{\text{filter},i}$ and $I_{\text{ideal},i}$ represent the measured transmitted power of the ith filter and the calibrated power of the corresponding ideal filter. In our approach, we use a simple algorithm

to estimate the coefficient matrix $[A]^{-1}$. Assuming we know the spectra of the first $i-2$ ideal filters, we can perform the following correction to the spectrum of the ith filter and estimate the spectrum of the ith ideal filter:

$$f^{1}_{\text{filter},i}(\lambda) = f_{\text{filter},i}(\lambda) - \frac{f_{\text{filter},i}(\lambda_1)}{f_{\text{ideal},1}(\lambda_1)} f_{\text{ideal},1}(\lambda),$$

$$f^{2}_{\text{filter},i}(\lambda) = f^{1}_{\text{filter},i}(\lambda) - \frac{f^{1}_{\text{filter},i}(\lambda_2)}{f_{\text{ideal},2}(\lambda_2)} f_{\text{ideal},1}(\lambda),$$

$$\cdots$$

$$f^{i-2}_{\text{filter},i}(\lambda) = f^{i-3}_{\text{filter},i}(\lambda) - \frac{f^{i-3}_{\text{filter},i}(\lambda_{i-2})}{f_{\text{ideal},i-2}(\lambda_{i-2})} f_{\text{ideal},i-2}(\lambda),$$

$$f_{\text{ideal},i}(\lambda) \approx f^{i-2}_{\text{filter},i}(\lambda). \quad (5)$$

The above equations mean that the side band intensity of the ith filter at the peak wavelength of the jth ideal filter λ_j has been subtracted to zero. $f^{j}_{\text{filter},i}(\lambda)$ represents the corrected spectrum of the ith filter after subtracting the spectra of 1st to jth ideal filters. The spectrum of the nearest neighboring ideal filter is not included in the correction, because of large overlap in spectral bandwidth. Thus, the corrected spectrum $f^{i-2}_{\text{filter},i}(\lambda)$ would be a good estimation of the ideal filter $f_{\text{ideal},i}(\lambda)$. Our first two filters can be treated as ideal filters, because their side bands are outside of our desired bandwidth and can be filtered out by a long pass filter. Then, based on the above method, we can suppress the side bands at shorter wavelengths to the main peaks of filters. Similarly, we can also improve the spectra at longer wavelengths, even though there is no side band at longer wavelengths. Finally, we get the estimated spectra of all ideal filters and coefficient matrix $[A]^{-1}$. The performance of our on-chip spectrometer is mainly determined by the characteristics of the main transmission peaks of the filters. Figure 3(a) plots the corrected transmission spectra of 28 filters. The influence of the side peak has been significantly suppressed. The filter efficiency ranges from 71% to 81%, and the FWHM varies from 7 nm to 13 nm. It is worth mentioning that we designed the filter array only targeting the first overtone of C-H stretch absorption band in the NIR wavelength range; however, our proposed on-chip spectrometer can apply to much wider bandwidth in NIR.

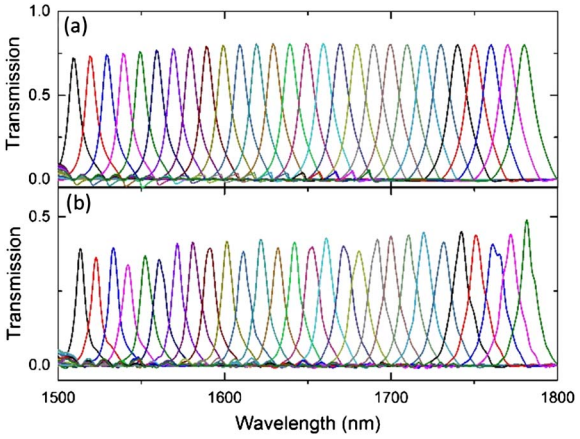

Fig. 3. (a) Simulated spectra of 28 designed filters after data correction covering the wavelength from 1510 nm to 1780 nm. (b) Calibration spectra of the fabricated filters after data correction.

An on-chip plasmonic spectrometer has been fabricated. First, a Cr (3 nm)/Au (40 nm) film is deposited on the quartz substrate through thermal evaporation. The purpose of the Cr layer is to improve the adhesion of the Au film to the substrate. Next, 28 filters are patterned through focused-ion beam (FIB) lithography. The dimension of each filter is 100 μm × 100 μm, large enough to minimize the aperture diffraction effect [32]. The spacing between each filter is 150 μm, which is sufficiently far away to eliminate the coupling between adjacent filters, which gives rise to a footprint of the total filter array around 1.5 mm^2, as is shown in Fig. 1(c). In the real device, more filters are fabricated for backup. Finally, 1.35 μm SU-8 photoresist is spun on the sample, cured by UV light, and hard baked under 95°C for 30 min.

Then, the optical properties of the fabricated filter array are characterized. A super-K compact supercontinuum light source (NKT Photonics, Denmark) is used as a broadband input. The output light from the light source is collimated and normally incident onto the sample from the substrate side after passing through a 1500 nm long-pass filter. A glass wafer with an anti-reflection layer at 1.55 μm is bonded to the substrate by index matching fluid to eliminate the interference from reflection. The beam size of the incident light is about 3 mm, which can cover the entire area of the filter array. On the other side, the transmitted light is directly coupled into a multi-mode fiber (MMF) with core diameter of 50 μm. Then, the MMF is connected to a Fourier transform IR spectrometer (OSA203, Thorlabs) to measure the transmission spectrum. Because the power density of each plasmonic filter is very uniform, the whole system has quite a large tolerance to optical coupling. Figure 3(b) shows the experimental results of the filters after performing the side band suppression method as described before. The transmission spectra are normalized to the optical power coupled into the same MMF through a bare quartz substrate with the same thick SU-8 cover layer using the same setup. The measured spectra exhibit a good match with the simulation results except minor bumps at 1750–1800 nm wavelength, possibly due to nonideal functions of the anti-reflection layer. The FWHM of each filter ranges from 7 nm to 13 nm, corresponding to the relative bandwidth from 0.46% to 0.73%. The peak position is slightly shifted from –0.5–2.0 nm due to the fabrication imperfections. The peak intensity of different filters is quite uniform, measured from 34% to 48%. At longer wavelengths, the anti-reflection layer does not work perfectly; small bumps are observed possibly due to the weak FP effect of the glass substrate. The filters only permit the transmission of TM-polarized light wave, and reflect the TE polarized light just like a planar gold film. Because no polarizer is used in our setup and the transmitted light intensity is normalized to the nonpolarized incident light, the transmission is underestimated by a factor of 2, which means the efficiency of our fabricated filters is comparable to the simulation results. Figure 4 shows the IR image of a row of filters taken by an IR CCD camera (A6200SC, FLIR) with a 20 × objective lens, when different narrow-band light waves (1 nm) from a monochromator are normally incident onto our device. The central wavelength marked in Fig. 4 corresponds to the peak wavelength of each filter.

In our experimental work, we used the on-chip spectrometer to measure the NIR absorption spectra of xylene. The incident light is chopped at 200 Hz by a mechanical chopper. For

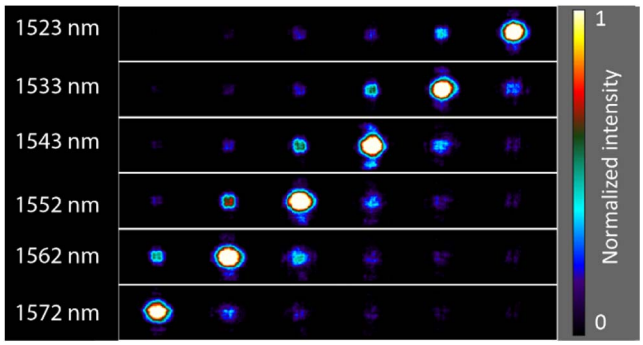

Fig. 4. IR images of one row of the plasmonic filters under normal incident of light with different wavelengths.

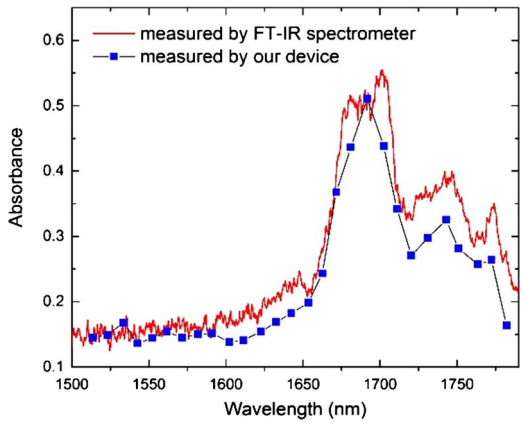

Fig. 5. Absorbance spectrum of xylene in 1 mm light path quartz flow cell, measured by FT-IR spectrometer (red solid) and by our device (blue square).

practical applications, the FT-IR spectrometer is replaced by an AC-coupled PbS amplified photoconductive detector (PDA30G, Thorlabs) connected to an oscilloscope and is synchronized to the chopper frequency. The xylene sample is filled into a quartz flow cell with 1 mm light path and is placed before the filter array. Each measurement is averaged in 1 s to improve the signal-to-noise ratio. The transmitted power of the filters is calibrated based on the previous side band suppression method to obtain the spectroscopy information. Figure 5 shows the NIR absorption spectra measured by our on-chip spectrometer and the commercial FT-IR spectrometer. The main absorption peak from 1680 nm to 1702 nm and side peaks at 1745 nm and 1773 nm, which correspond to the first overtones of the aromatic C-H-stretching vibrations and the methyl vibrations in xylene [33], are clearly resolved by our on-chip spectrometer and matches the FT-IR measurement results quantitatively.

In short, we have designed and experimentally demonstrated a 28-channel on-chip spectrometer at the NIR range based on an array of narrow-band plasmonic filters, providing FWHM around 10 nm and operation bandwidth over 270 nm. The on-chip spectrometer has the advantages of ultra-compact size, high throughput if used with an IR camera, and high reliability as it is free of any moving mechanical component, which shows great potential for portable IR spectroscopy systems for a variety of future applications.

Funding. National Science Foundation (NSF); Directorate for Engineering (ENG) (1342318, 2841449383); National Institute of Biomedical Imaging and Bioengineering (NIBIB) (1R03EB018893, 9R42ES024023).

REFERENCES

1. C. Elosua, I. R. Matias, C. Bariain, and F. J. Arregui, Sensors **6**, 11 (2006).
2. R. Magnusson, D. Wawro, S. Zimmerman, Y. Ding, M. Shokooh-Saremi, K. J. Lee, D. Ussery, S. Kim, and S. H. Song, Proc. SPIE **7604**, 76040M (2010).
3. A. Nitkowski, L. Chen, and M. Lipson, Opt. Express **16**, 11930 (2008).
4. W.-C. Lai, S. Chakravarty, X. Wang, C. Lin, and R.-T. Chen, Appl. Phys. Lett. **98**, 023304 (2011).
5. R. Gordon, D. Sinton, K. L. Kavanagh, and A. G. Brolo, Acc. Chem. Res. **41**, 1049 (2008).
6. C. F. Carlborg, K. B. Gylfason, A. Kaźmierczak, F. Dortu, M. B. Polo, A. M. Catala, G. M. Kresbach, H. Sohlström, T. Moh, L. Vivien, and J. Popplewell, Lab Chip **10**, 281 (2010).
7. R. Adato and H. Altug, Nat. Commun. **4**, 2154 (2013).
8. H. W. Siesler, Y. Ozaki, S. Kawata, and H. M. Heise, *Near-Infrared Spectroscopy* (Wiley, 2008).
9. M. Lackner, Rev. Chem. Eng. **23**, 65 (2007).
10. T. Fukazawa, F. Ohno, and T. Baba, Jpn. J. Appl. Phys. **43**, 646 (2004).
11. K. Kodate and Y. Komai, J. Opt. A **10**, 044011 (2008).
12. N. Yebo, W. Bogaerts, Z. Hens, and R. Baets, IEEE Photon. Technol. Lett. **23**, 1505 (2011).
13. S. Janz, A. Balakrishnan, S. Charbonneau, P. Cheben, M. Cloutier, K. Dossou, L. Erickson, M. Gao, and P. A. Krug, IEEE Photon. Technol. Lett. **16**, 503 (2004).
14. X. Ma, M. Li, and J. He, IEEE Photon. J. **5**, 7101307 (2013).
15. B. Momeni, E. S. Hosseini, M. Askari, M. Soltani, and A. Adibi, Opt. Commun. **282**, 3168 (2009).
16. Z. Xia, A. A. Eftekhar, M. Soltani, B. Momeni, Q. Li, M. Chamanzar, S. Yegnanarayanan, and A. Adibi, Opt. Express **19**, 13 (2011).
17. R. F. Wolffenbuttel, IEEE Trans. Instrum. Meas. **53**, 197 (2004).
18. S.-W. Wang, C. Xia, X. Chen, W. Lu, M. Li, H. Wang, W. Zheng, and T. Zhang, Opt. Lett. **32**, 6 (2007).
19. W. L. Barnes, A. Dereux, and T. W. Ebbesen, Nature **424**, 824 (2003).
20. R. Magnusson and S. S. Wang, Appl. Phys. Lett. **61**, 1022 (1992).
21. Y. Ding and R. Magnusson, Opt. Express **12**, 23 (2004).
22. F. Ren, M. Li, Q. Gao, W. Cowell, J. Luo, A. K. Jen, and A. X. Wang, Opt. Commun. **352**, 116 (2015).
23. J.-N. Liu, M. V. Schulmerich, R. Bhargava, and B. T. Cunningham, Opt. Express **22**, 15 (2014).
24. R. R. Boye and R. K. Kostuk, Appl. Opt. **39**, 3649 (2000).
25. T. Xu, Y. K. Wu, X. Luo, and L. J. Guo, Nat. Commun. **1**, 59 (2010).
26. A. F. Kaplan, T. Xu, and L. J. Guo, Appl. Phys. Lett. **99**, 143111 (2011).
27. Q. Chen and D. R. Cumming, Opt. Express **18**, 13 (2010).
28. S. Yokogawa, S. P. Burgos, and H. A. Atwater, Nano Lett. **12**, 4349 (2012).
29. D. B. Mazulquim, K. J. Lee, J. W. Yoon, L. V. Muniz, B. H. Borges, L. G. Neto, and R. Magnusson, Opt. Express **22**, 30843 (2014).
30. J. M. Steele, C. E. Moran, A. Lee, C. M. Aguirre, and N. J. Halas, Phys. Rev. B **68**, 20 (2003).
31. J. M. McMahon, J. Henzie, T. W. Odom, G. C. Schatz, and S. K. Gray, Opt. Express **15**, 18119 (2007).
32. F. Ren, K. Y. Kim, X. Chong, and A. X. Wang, Opt. Express **23**, 22 (2015).
33. J. Workman, Jr. and L. Weyer, *Practical Guide to Interpretive Near-Infrared Spectroscopy* (CRC Press, 2007).